Molecular dynamics simulations of microstructural evolution of irradiated (U,Pu)O2 studied via simulated XRD patterns

Alain Chartier, Paul Fossati, Laurent van Brutzel

Version of Record: https://www.sciencedirect.com/science/article/pii/S0022311522003208
Manuscript_9b9441be33e596e8c6980a2f885a6754

Molecular dynamics simulations of microstructural evolution of irradiated $(U,Pu)O_2$ studied via simulated XRD patterns

Laurent Van Brutzel[a,*], Paul Fossati[a], Alain Chartier[a]

[a] *Université Paris-Saclay, CEA, Service de la Corrosion et du Comportement des Matériaux dans leur Environnement, 91191, Gif-sur-Yvette, France*

Abstract

Molecular dynamics simulations of microstructural evolution under irradiation of $(U,Pu)O_2$ solid solutions have been carried out with the Frenkel pair accumulation method with two empirical potentials. Simulated X-Ray diffraction patterns have been systematically generated along the irradiation pathway from the computed atomistic configurations. Description of the X-Ray diffraction patterns for each of these well characterized damage microstructure snapshots is discussed. Attempt to correlate the features of the X-Ray diffraction peaks with the microstructural evolution with irradiation dose is also provided. Special attention is dedicated to the swelling effect.

Keywords: Molecular dynamics, MOX fuel, irradiation, XRD pattern

1. Introduction

Mixed oxide nuclear fuel (MOx), composed primarily of uranium and plutonium oxide, provides a significant percentage of the nuclear fuel used

*Corresponding author. Tel.: +33-169087915; Fax: +33-169089221
Email address: laurent.vanbrutzel@cea.fr (Laurent Van Brutzel)

in new Pressurized Water Reactors or in envisaged future Generation IV nuclear plants. During its lifetime in these reactors, it undergoes chemical, structural, and physical changes due mainly to high thermal gradient and irradiation. One of the most important property which influences safety and fuel design is the swelling effect. This increase in volume of the fuel occurs under irradiation and is usually attributed to the creation of defects such nanocavities or accumulation of fission products. To study this behaviour, direct analysis of the sample density or X-Ray diffraction (XRD) are usually carried out. Several XRD studies in UO_2 confirmed that lattice parameter and microstrain increase with the increasing dose [1–5]. However, XRD pattern interpretation can be sometimes controversial due to the complexity of the burnup fuel system. Moreover, heavy ions external irradiation techniques on pristine fuel leads usually to a thin irradiated surface and an undefected material underneath. For this type of sample, XRD analysis is difficult to deconvolve.

Recently, combination of experimental XRD results and Molecular Dynamic Simulations (MD) [6, 7] helps to sort out the different defect contributions of the XRD patterns in SiC and ZrC. In this article the authors endeavour to deconvolve the elastic strain obtained from XRD with the different defect contributions calculated from molecular dynamics simulations. These atomistic simulations provide the microstructure evolution as a function of the increasing dose via Frenkel pair accumulation method [11, 12]. This method, consists on the accumulation of Frenkel pairs at regular time intervals, which can recombine or reorganize into more complex extended defects such as dislocation or nanocavity within a very short time. It thus

probes the microstructure evolution created during the spontaneous defect reorganization regime.

In UO_2 Chartier *et al.* [8] and Jin *et al.* [5, 9] also attempt, using the same method, to deconvolve the global lattice parameter evolution as a function of irradiation dose with the different defect contributions. However, in these last studies the defects from the oxygen sub-lattice were not taken into account and relaxation volume for the uranium vacancy has to be hypothesis positive in order to fit the experimental results, which is in contradiction with ab-initio calculations [10].

Following these studies, the same methodology is invoked herein to investigate simulated XRD patterns from several well-characterized damaged $(U,Pu)O_2$ solid solutions. The damaged configuration snapshots are created with the Frenkel pair accumulation method. Each configuration is rigorously analysed and XRD patterns are systematically calculated using the Debye scattering equation with the corresponding atomic coordinates. This database of XRD patterns with corresponding well-defined damaged microstructures can help the deconvolution and interpretation of experimental XRD patterns from real physical systems. Furthermore, correlation between the microstructure evolution in both cation and anion sub-lattices and the simulated XRD patterns is also discussed.

The paper is organized as follow: section 2 describes briefly the methodology employed to irradiate the $(U,Pu)O_2$ solid solution and simulated the associated XRD patterns, section 3 describes the simulated XRD patterns and subsequently discusses the correlation between the microstructural evolution and the XRD pattern changes as a function of the increasing dose.

2. Computational method

2.1. Potential interactions

For this study we used Molecular Dynamics simulations to simulate the evolution of the microstructure of (U,Pu)O_2 solid solution under increasing radiation damage. All simulations have been performed via the LAMMPS code [13]. The study herein concerns three (U,Pu)O_2 compositions: pure uranium dioxide (UO_2), a mix with 50% uranium atoms ($U_{0.5}Pu_{0.5}O_2$), and pure plutonium dioxide (PuO_2). It is known experimentally that the ternary system $U_{1-x}Pu_xO_2$ forms an ideal solid solution for the full range of Pu content and from room temperature to nearly melting point [14]. Therefore, for the mix, the initial positions of the cations are randomly distributed into the regular sites of the face-centered structure. All the initial structures are the fluorite structure of space group F$m\bar{3}m$. The system box size is $22 \times 22 \times 22$ nm^3, involving 768 000 atoms.

MD simulations rely on the quality of the interatomic potential for accurate results; hence, we have investigated systematically two interatomic potentials, in order to compare and contrast the results and estimate the errors due to the interatomic models. The first set of potentials have been developed by Potashnikov and al. [15] and will be referenced herein as MOX-07. Previous studies assessed thermodynamics and transport properties as well as point defect formation energies for these potentials [16, 17]. The results are in good agreement with experimental data however, they slightly underestimate the bulk and shear moduli and show isotropic behaviour for the elastic stiffness with a Zener's ratio close to 1. This is due to the fact that these potentials have been fitted with experimental data coming from

polycrystal samples. The second set of potentials used herein have been developed by Cooper *et al.* [18, 19] and will be coined CRG. These potentials provide also really good thermodynamic and transport properties as well as mechanical properties with anisotropic behaviour for the elastic stiffness. This potential reproduces also accurately the thermal conductivity and heat capacity, which are related to anharmonic effects [20]. However, they yields to metastable configurations under irradiation in the oxygen sublattice, which imposes longer simulations before stability is reached [17]. This made them less handy to use for irradiation studies.

The long-range Coulombic interactions is calculated via the particle-particle/particle-mesh (PPPM) method provided in the LAMMPS code [21].

2.2. Modelling irradiation dose

At the atomistic length scale, irradiation events lead mainly to electronic excitation but also to the creation of point defects such as vacancies or interstitials. As the irradiation dose increases, these point defects accumulate and aggregate to change the microstructure. It is these changes that we are trying to describe with MD simulations. Usually in MD simulations, irradiation damage is performed by modelling displacement cascades. This type of simulation is computationally expensive but gives a fairly good description of the full process of an irradiation event including the thermal spike and the structural recovery. However, it describes only the primary damage of one single event, which mainly consists in the case of MOx fuel of few point defects as shown in previous studies [17]. Therefore, in order to study the dose effect (accumulation of damage), we use an alternative method: the Frenkel Pair Accumulation Method (FPA) [11, 12]. This method consists

on introducing periodically and consistently Frenkel pair defects, while the structure is continuously allowed to relax under constant pressure and temperature. Here, the introduced Frenkel pairs mimic the remaining damage after displacement cascades. In that respect, this method corresponds to the accumulation of the final stage of displacement cascades within the same volume.

Previously Chartier *et al.* [8] showed that the oxygen sublattice seems to follow the cation disorder. Consequently, only cation Frenkel pairs (C-FP) are introduced in order to reduce the computational time. The time interval between two subsequent C-FP introductions is set to 2 ps. This time is large enough to allow spontaneous C-FP recombination, which has no dependence with the temperature and for which the distance between the vacancy and the interstitial is up to 1.5 nm corresponding to the 5^{th} cation nearest-neighbour [16, 22]. We have checked that within the time-lapse between two FP introductions the temperature and pressure of the system reach the desired values and that just expected thermal fluctuation occurs. The system is then considered stabilized enough to permit the introduction of the next set of defects. All the simulations have been carried out at room temperature (300 K) and 0 GPa. Due to the high increase in energy arising from each FP introduction, the NPT relaxation for this FPA procedure is done with the Berendsen algorithm provided by the LAMMPS code [23].

Each C-FP introduction sequence involves the creation of 700 FPs for the MOX-07 potential and 300 for the CRG potential within the simulation box. Because the defect recombination time is higher for CRG potential, less FPs can be introduced within the same time interval. It is also worth noticing

that this number corresponds approximatively to the remaining number of Frenkel pairs remaining after a displacement cascade simulation initiated with a primary knock-on atom energy of 80 keV [17].

A common way to measure irradiation dose on materials is the use of displacements per atom (dpa). This is also a very simple metric from the atomistic simulations point of view. It is defined simply by the number of displacements (on average) of one atom, which exactly corresponds to what is simulated with the FPA method. Since in our study only C-FPs are created, we express the dose in displacements per cation (MD-dpc) rather than the classic dpa. Therefore, for each C-FP introduction, the dose is increased by 1.17×10^{-3} MD-dpc and 2.73×10^{-3} MD-dpc for CRG and MOX-07 potentials respectively. It is worth noting that this unit of dose does not correspond directly to the experimental dpa unit of dose, which is usually calculated via SRIM calculations. Straight quantitative comparison between both units should not be considered. Nonetheless, increasing MD-dpc indicates that the number of displaced atoms increases and hence that the irradiation dose increases as well.

The analysis of the structural evolution is carried out using OVITO software [24]. We determined the dislocation density with the DXA algorithm provided in OVITO and examined the point defects with a fine structural detection via a homemade software, ACME [25]. This last method was chosen over the Wigner-Seitz or the Voronoi cell analysis because numerous disoriented fluorite subdomains appear during the simulation.

2.3. Simulated XRD pattern

Beside the analysis of the point defects and the dislocations, we are generating simulated X-Ray powder diffraction (XRD) patterns via the Debyer software [26] from irradiated configurations. During the FPA procedure, sampling of irradiated configurations are saved. These configurations are systematically relaxed for 20 ps under constant temperature (300 K) and constant pressure (0 GPa) with the Parrinello and Rahman algorithm [27] in order to further anneal the system and eliminate any residual unstable defects. Subsequently, the simulated XRD patterns are calculated with the atomic coordinates averaged over the last 5 ps of the relaxation. The defect analysis is also carried out at this stage. XRD patterns are calculated simply using the Debye scattering equation:

$$I(Q) = \sum_i \sum_j f_i f_j \frac{\sin(Q r_{ij})}{Q r_{ij}} \tag{1}$$

where Q is the scattering vector defined as: $Q = |\boldsymbol{Q}| = 4\pi \sin\theta/\lambda$, where θ is the diffraction half-angle and λ is the wavelength, ($\lambda = 1.5406$ Å). $r_{ij} = |\boldsymbol{r}_i - \boldsymbol{r}_j|$ is the distance between atoms i and j, and f_i is the atomic scattering factor of the i^{th} atom.

Because our simulation uses periodic boundary conditions ("infinite" bulk material) a cut-off radius is applied to limit the number of atomic pairs accounted in the Debye formula. Only pairs with distances inferior to this radius are considered. However, a correction term is added to avoid large sinusoid. Therefore, the normalized intensity of the scattered wave becomes:

$$I(Q)/N = f^2 \Bigg\{ \frac{1}{N} \left[\sum_i \sum_{j, r_{ij} < R_c} \frac{\sin(Q r_{ij})}{Q r_{ij}} \right] + \frac{4\pi\rho}{Q^3} \Big[Q R_c \cos(Q R_c) - \sin(Q R_c) \Big] \Bigg\} \quad (2)$$

where R_c is the cut-off radius equals in our simulation to half the box size, *i.e.* 11 nm.

The resulting simulated XRD patterns are further analysed with Fityk software [28] in order to identify the feature of the different peaks. It appears that the best fit for the peaks in our simulated XRD pattern is Gaussian function.

3. Results and discussion

3.1. Microstructure evolution with irradiation dose

Before presenting the simulated XRD patterns as a function of the irradiation dose, it is important to describe the evolution of the microstructure and the nature of the associated damage with the irradiation dose. Figure 1 depicts the point defect evolution (vacancies and interstitials) and the dislocation density as a function of dose expressed in MD-dpc for the three Pu contents studied (0%, 50%, and 100%) at 300 K for the MOX-07 potentials. Likewise, Figure 2 depicts the same results for the CRG potential. To illustrate the type of damage created, snapshots of the simulation in UO_2 analysed with the DXA tool from OVITO are also displayed. As previously detailed for UO_2 [8] and for the $U_{1-x}Pu_xO_2$ solid solution [17] carried out at

1600 K, we show that the evolution of the microstructure in these materials mainly follows a five-stage process:

1. For doses lower than 0.2 MD-dpc, isolated point defects are first created. This is demonstrated by a rapid increase of the number of vacancies and interstitials (highlighted by the pink area in Figure 1 and Figure 2). It is noteworthy that within this stage the number of vacancies is equal the number of interstitials because only isolated Frenkel pairs are created.
2. Subsequently and up to 0.5 MD-dpc, for the MOX-07 potential the number of interstitials decreases rapidly while the number of vacancy continues to increase steadily. This indicates that most of the interstitials aggregate into clusters while the vacancies remain isolated. For CRG potential, UO_2 compounds follows the same behaviour. In the mix and pure PuO_2 the decrease of the interstitials is less pronounced yet still occurs while the number of vacancies seems to stabilize.
3. For the MOX-07 potential, the interstitial clusters nucleate mostly into Frank loops as demonstrated by the peak density of Frank loops highlighted in blue in Figure 2. For the CRG potential this stage seems to be skipped as almost no Frank loops are created.
4. Around 0.5 MD-dpc, for the MOX-07 potential the Frank loops transform into perfect dislocations whereas for the CRG potential the interstitial clusters form perfect dislocations directly.
5. Subsequently, for both potentials, the density of perfect dislocations decreases even if for the mix with CRG is less abrupt indicating in that case a growth of the small loops. After about 2 MD-dpc a steady

state is reached and dislocations reorganize into forest of dislocations creating few disoriented nanodomains.

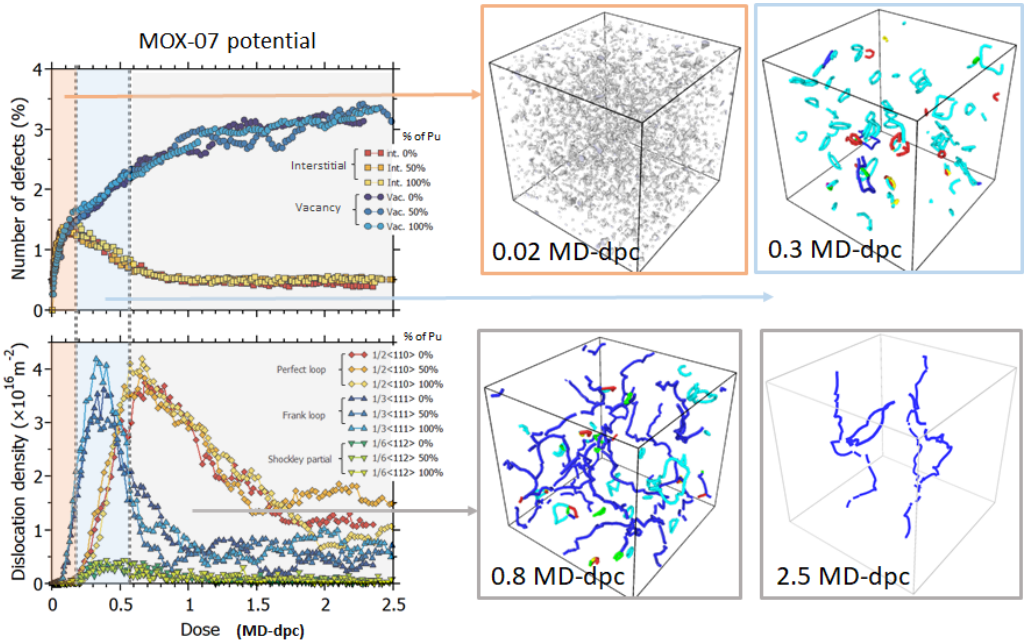

Figure 1: Evolution of the number of point defects and dislocation density as a function of dose for the MOX-07 potential at 300 K. Three snapshots of the simulation box of UO_2 analysed with the DXA tool from OVITO are also displayed to illustrate the damage. In these figures the grey dots at 0.02 MD-dpc represent the track of the point defects. For clarity only the dislocation lines are represented in the figure at 0.3, 0.8, and 2.5 MD-dpc (dark blue: perfect loop, cyan: Frank loops, green: Shockley partials, and red: Stair-Rod).

Even if there is a quasi-absence of Frank loops generation with the CRG potential the damage process evolution is roughly similar with both potentials. However, it is worth noticing that with CRG potential the Pu content has some influence. Namely, as the Pu content increases the total density of dislocation loops decreases and the peak in the dislocation density appears

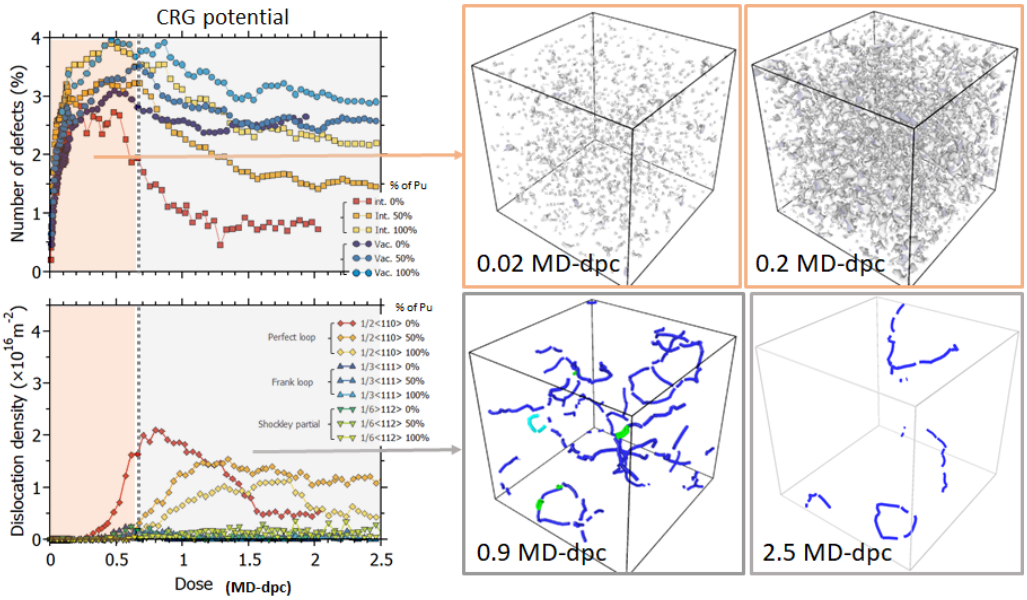

Figure 2: Evolution of the number of point defects and dislocation density as a function of dose for the CRG potential at 300 K. Three snapshots of the simulation box of IO_2 analysed with the DXA tool from OVITO are also displayed to illustrate the damage. In these figures the atoms in fluorite crystallographic position are removed for clarity. The grey dots at 0.02 and 0.2 MD-dpc represent the track of the point defects. In the last two snapshots at 0.9and 2.5 MD-dpc only the dislocation lines are represented for clarity (dark blue: perfect loop, cyan: Frank loops, green: Shockley partials).

for higher dose. This could indicate either that the formation of dislocation loops is easier with low Pu content or that with this potential the characteristic time for the formation of dislocation loops assisted by spontaneous reorganization of defects is slower.

In the following this five-stage process will be reduced into three main domains of microstructures. The first one from 0 to 0.2 MD-dpc highlighted in pink in figures denotes the isolated point defects microstructure, the sec-

ond one appearing only with the MOX-07 potential from 0.2 to 0.5 MD-dpc highlighted in blue represents the microstructure dominated by Frank loops, and the third one from 0.5 to 2.5 MD-dpc highlighted in light grey designated microstructures containing mainly perfect dislocations. It is important noticing that in this last microstructure numerous point defects, principally vacancies, are remaining. After analysing the spatial distribution of these vacancies, we found that 50% of the vacancies are isolated (mono-vacancy) however about 25% form bi- or tri-vacancy clusters. The remaining 25% is distributed among larger clusters that could include more than 30 vacancies for both potentials forming nanocavities.

The damaged microstructures is here generated by the reorganization of close defects over a very short time-scale. This microstructural evolution, considered as spontaneous, involves sometime complex pathways that could be thermally activated. However, diffusion kinetics over long distances of extended defect, such as dislocations or nanocavities is out of reach with the time frame of the MD simulations. Nevertheless, simple order-of-magnitude calculation based on the characteristic distance between displaced atoms estimated from typical dose rate compared to characteristic self-diffusion distance shows that defects anneal mainly by close defect interactions. As a matter of fact, characteristic distance between two displaced atoms can be determined by $d = (V_{at}/K)^{1/3}$, where V_{at} is the atomic volume (13.6 Å in MOx) and K is the dose rate (typically around 10^{-3} dpa.s^{-1}). This distance within one second is equal to approximately 3 nm. On the other hand, cation irradiation-induced solid-state diffusion is generally taken from Matzke recommendation [29] and is expressed as: $D = 1.2 \times 10^{-39}.\dot{F}$ m^2.s^{-1}, where $\dot{F}$ is

the fission rate. Fission rate calculated by T. Sekine et al. [30] using Monte-Carlo simulations in MOx fuel ranges from 10^{11} to 10^{14} fission.m^{-3}.s^{-1}. This yields to diffusion coefficient close to $D = 1.2 \times 10^{-25}$ m^2.s^{-1}, for the highest. The cation characteristic distance travelled by diffusion within one second is then approximatively equal to 0.003 nm, which is a thousand times smaller than the characteristic distance between defects. Therefore, recombination regime handled by our MD simulations plays a significant role on the formation of the damaged microstructure. Consequently, the damaged structural configurations studied herein should be representative of some first stage damages of the real system.

3.2. Simulated XRD patterns

As mentioned above, for each configuration saved and relaxed as the irradiation dose increases a simulated XRD pattern is generated with the Debyer software. About a hundred configurations are investigated for each compound and for both interatomic potentials. The XRD patterns are generated for diffraction angles from $2\theta = 20°$ to $2\theta = 90°$. As an illustration of these results, figures 3(a) and 3(b) display 3D plots of the simulated XRD patterns in UO_2 as a function of dose in MD-dpc from configurations calculated with the MOX-07 and the CRG potential respectively.

Overall, the main behaviour of the XRD patterns is the same for both interatomic potentials. All the XRD patterns are rather well defined without any background noise, which eases the analysing of the peaks. No change of phase is found as the irradiation dose increases. However, changes appear in the intensity, the full width at half maximum (FWHM), and in the position of the peaks, *i.e.* the diffraction angle for the peak maxima.

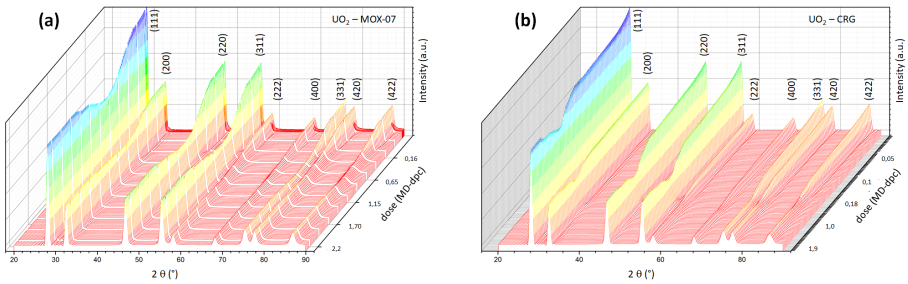

Figure 3: 3D representations of the simulated XRD patterns of UO_2 as a function of irradiation dose from configurations calculated with (a) MOX-07 potential and (b) CRG potential. It is worth noticing that the scale for the doses is not linear.

To illustrate more precisely these changes, the relative intensity defined as the intensity at a certain dose divided by the intensity of the pristine material (*i.e.* I(MD-dpc)/I(0)) for the most intense peak at the Miller indices (1 1 1) is reported in figure 4(a) for all the compounds and for both empirical potentials. For all the compounds calculated with MOX-07 and for UO_2 calculated with CRG, the diffraction peaks intensity decreases as the irradiation dose increases until approximatively 0.5 to 0.7 MD-dpc before increasing back and reaching a plateau. For $U_{0.5}Pu_{0.5}O_2$ and PuO_2 calculated with CRG, the intensities decrease and reach a plateau around 1.2 MD-dpc like the others compounds.

An other interesting feature of the peaks is the evolution of the FWHM, which is reported in figure 4(b). Peak broadening in the case of one phase single crystal usually indicates microstrains, which are related to the formation of defects in the crystal structure such as dislocation or stacking faults. For this feature, we observe an increase and a drop with a maximum around 0.6-0.7 MD-dpc followed by a plateau at around 1.5 MD-dpc for all the com-

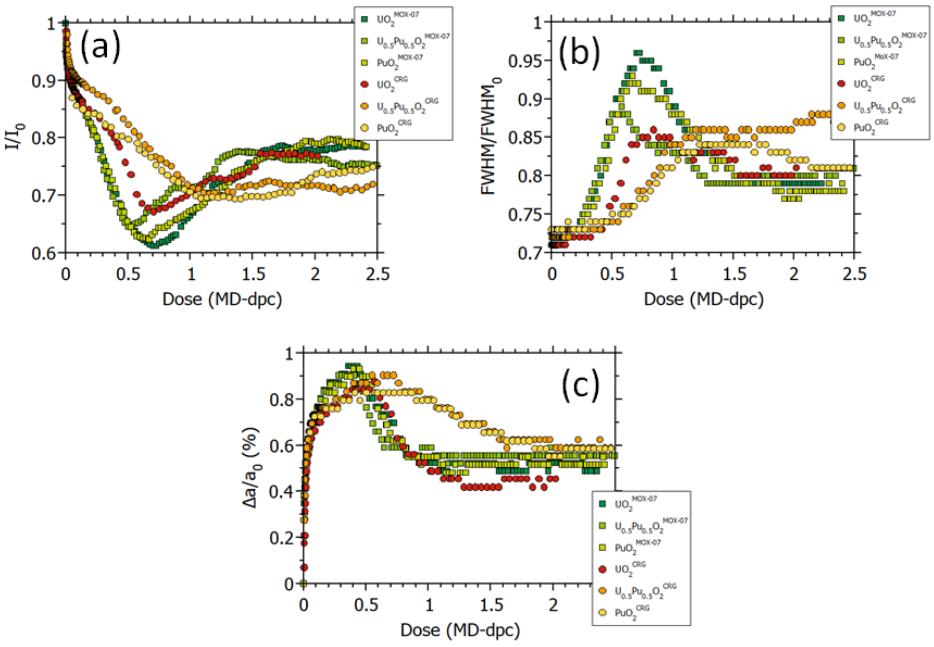

Figure 4: Evolution as a function of irradiation dose of (a) the relative intensity (I(MD-dpc)/I(0)), (b) the relative full width at half maximum (FWHM(MD-dpc)/FWHM(0)), and (c) the relative lattice parameter (a(MD-dpc)-a(0))/a(0)) calculated of the peak of Miller indices (1 1 1) for UO_2, MOx ($U_{0.5}Pu_{0.5}O_2$), and PuO_2 calculated with both empirical potentials.

pounds calculated with MOX-07 and UO_2 calculated with CRG. Conversely, for $U_{0.5}Pu_{0.5}O_2$ and PuO_2 calculated with CRG, the FWHM increases till about 1.2 MD-dpc where it plateaus.

The evolution of the relative lattice parameter calculated from the first most intense peak at the Miller indices (1 1 1) is reported in figure 4(c). The relative lattice parameter is defined as [a(MD-dpc)-a(0)]/a(0), where a(MD-dpc) is the lattice parameter at a given irradiation dose. The lattice parameter for a given irradiation dose is calculated with the following

equation:

$$a(hkl) = \frac{\lambda\sqrt{h^2+k^2+l^2}}{2\sin(\theta/2)} \tag{3}$$

where λ is the wavelength and hkl the Miller indices of the peak, here $\sqrt{h^2+k^2+l^2} = \sqrt{3}$. This quantity can be directly related to the swelling of the material. Conversely to the relative intensity, all the lattice parameter first increases to reach a maximum then drops to a plateau at higher doses. This means that the material initially swells before shrinking and then stabilizes but yet to a lattice parameter higher than its original parameter. The maximum of swelling is found for the compounds calculated with MOX-07 around 0.4 MD-dpc. For those calculated with CRG, the maximum is observed around 0.6 to 0.7 MD-dpc. For $U_{0.5}Pu_{0.5}O_2$ and PuO_2 the relative lattice parameters decrease like for the other system However, it decreases at a slower rate reaching its plateau around 1 MD-dpc.

Overall, the main behaviour of the simulated XRD pattern is similar for both potentials, even if with the CRG potential the Pu content is much more pronounced.

3.3. Correlation with microstructure evolution

All these features are interesting because they show that the evolution with the increasing dose is rather complex with probably different microstructure influence. In the following, we will try to correlate these behaviours with the microstructural evolution involved in our simulated irradiated systems.

After some investigations, it appears clearly that the FWHM features are directly correlated with the evolution of the perfect dislocation loops (Burger's vector: b=a/2$\langle 1\,1\,0\rangle$). To illustrate this hypothesis, we plot on the

same graph in figure 5 the FWHM and the density of dislocation loops as a function of irradiation dose. For clarity, the results calculated from both empirical potentials are displayed in two different figures: 5(a) for MOX-07 and 5(b) for CRG. In these figures the curves of the perfect dislocation density follow the exact shape of the FWHM curves for both potentials. Differences only appear on the relative amplitude for the $U_{0.5}Pu_{0.5}O_2$ compounds for both potentials and for PuO_2 with the CRG potential. It also appears that there is no correlation with the Frank loop density for the compound calculated with MOX-07. For compounds calculated with CRG, the Frank loop density is very small; hence comparison is difficult. However, this behaviour indicates that the broadening of the simulated XRD peaks are mainly due to the presence of microstrains generated by perfect dislocations surrounding the disorientated nanodomains. As the irradiation dose increases, the number of perfect dislocation segments decrease resulting in the diminution of the number of nanodomains but an increase of their size. Indeed, at the highest irradiation dose only a few nanodomains remain, separated by few long lines of perfect dislocations (see figure 1 and figure 2 at 2.5 MD-dpc). This microstructure evolution toward fewer defects of nanometre size yields to the release of the local strain and subsequently to sharpener peaks into the simulated XRD patterns.

For intermediate irradiation doses (*i.e.* 0.4-0.5 MD-dpc), new small peaks appear in the simulated XRD patterns calculated with the MOX-07 potentials. An example of this pattern is displayed in figure 6(a) where the extra small peaks are underlined with arrows. They are all located to the right of the classical peaks of the fluorite structure. After investigation, these peaks

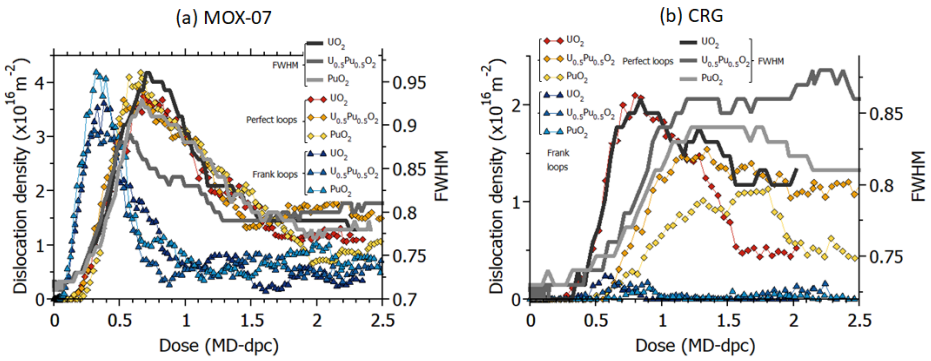

Figure 5: Evolution as a function of irradiation dose of the density of dislocation loops and fwhm calculated from the (1 1 1) peaks of the simulated XRD patterns for (a) compounds calculated with MOX-07 and (b) compounds calculated with CRG.

do not appear as artefacts of the simulation but seem rather directly correlated with the density of Frank loops. In figure 6(b), we reported on the same graph the maximum intensity of the new peak at around $2\theta = 29°$ corresponding to the first arrow in the figure 6(a) and the evolution of the dislocation densities for both Frank loops and perfect loops. The intensity of this new peaks follows almost perfectly the shape of the Frank loop densities for all the compounds. It is also important to notice that no new peak is detected on the simulated XRD patterns calculated with the CRG potential for which very few Frank loops are found. Since these new peaks follow the regular fluorite peaks, they could be interpreted as a fluorite-like structure with a smaller lattice parameter (*e.g.* for the configuration in figure 6(a), the lattice parameter of the small peaks is approximatively equal to $a = 5.3$ Å instead of $a = 5.5$ Å for the regular peaks.). These fluorite-like structures could then correspond to the structure inside a Frank loop, which is more

366 constrained than in the bulk leading to smaller lattice parameter.

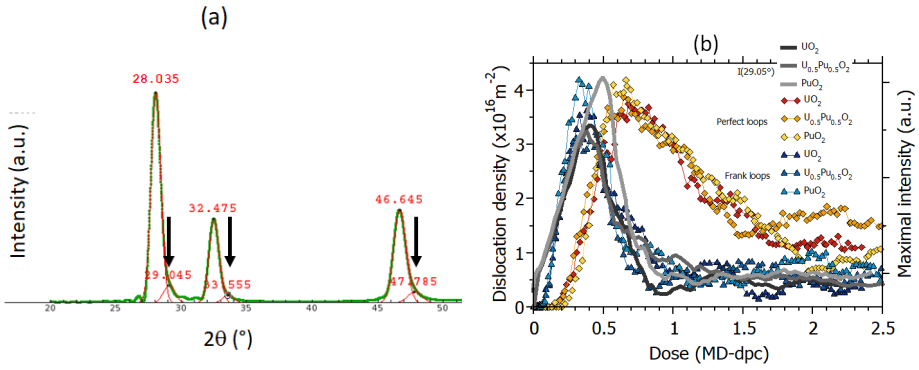

Figure 6: (a) Close up of the simulated XRD pattern of UO_2 calculated with MOX-07 potential at 0.4 MD-dpc. The arrows indicate the position of the new peaks found for this configuration. (b) Evolution as a function of irradiation dose of the density of dislocation loops and the maximum intensity of the new peak at around $2\theta = 29°$ corresponding to the first arrow in the figure 6(a).

367 Another interesting feature that can be analysed from XRD pattern is the
368 evolution of the lattice parameter, which gives an indication of the swelling
369 of the material under irradiation. We already computed the evolution of
370 the lattice parameter as a function of the increasing irradiation dose in fig-
371 ure 4(c). We now compare these graphs for UO_2 with the theoretical ex-
372 pansions derived from each defect relaxation volume contributions as the
373 following equation:

$$\frac{\Delta a}{a_0} = \frac{1}{3}\Bigg[C_{\text{int.}}(\text{U})\frac{V^{\text{rel}}_{\text{int.}}(\text{U})}{\Omega} + C_{\text{vac.}}(\text{U})\frac{V^{\text{rel}}_{\text{vac.}}(\text{U})}{\Omega} + C_{\text{int.}}(\text{O})\frac{V^{\text{rel}}_{\text{int.}}(\text{O})}{\Omega} + C_{\text{vac.}}(\text{O})\frac{V^{\text{rel}}_{\text{vac.}}(\text{O})}{\Omega}\Bigg] + \frac{\pi b^2}{4}\rho_{\text{perfect}} + \frac{b\bar{R}_{\text{Frank}}}{2}\rho_{\text{Frank}} \quad (4)$$

where $C_{\text{int.}}$ and $C_{\text{vac.}}$ are is the interstitial and the vacancy concentrations (respectively), V^{rel} is the relaxation volume of each defect expressed in atomic volume unit Ω, b is the Burger's vector associated to the type of loop (*i.e.* $b = a/\sqrt{2}$ for perfect loops and $b = a/\sqrt{3}$ for Frank loops), $\bar{\text{R}}_{\text{Frank}}$ is the average radius size of the Frank loops found in our simulation (2 nm), and ρ is the dislocation density expressed in m^{-2}. The defect concentrations and dislocation densities are directly calculated from the MD simulations, relaxation volumes of each defect are taken from the DFT calculations carried out by Bruneval *et al.* [10]. The values of all the relaxation volumes are reported in the table 1.

$\text{V}^{\text{rel}}_{\text{int.}}(\text{U})/\Omega$	$\text{V}^{\text{rel}}_{\text{vac.}}(\text{U})/\Omega$	$\text{V}^{\text{rel}}_{\text{int.}}(\text{O})/\Omega$	$\text{V}^{\text{rel}}_{\text{vac.}}(\text{O})/\Omega$
1.02	-0.23	0.02	0.175

Table 1: Relaxation volume of point defects calculated with DFT by Bruneval *et al.* [10] in UO_2.

Figure 7(a) and (b) report the comparison of the lattice parameter expansion as a function of irradiation dose between those found with the simulated XRD in UO_2 and the theoretical values calculated with the equation 4. Only

UO_2 compounds have been investigated because to our knowledge the relaxation volume of defects in MOx or PuO_2 have not been yet calculated. However, we hypothesis that their behaviour would follow the one of UO_2.

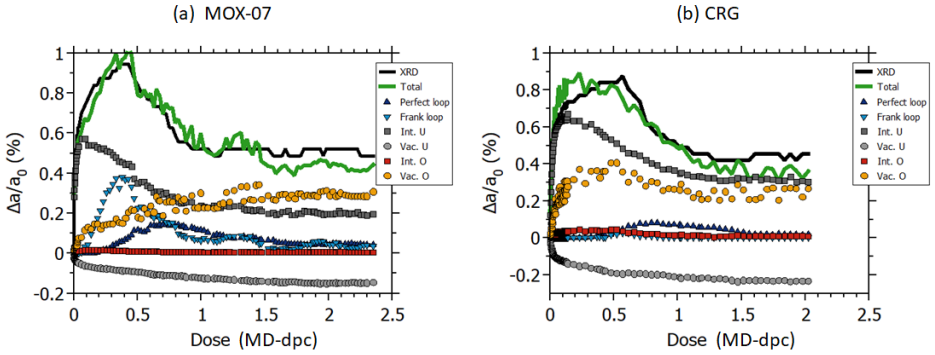

Figure 7: Theoretical contribution of the different defects to the relative lattice parameter [a(MD-dpc)-a(0)]/a(0) corresponding to the swelling as a function of irradiation dose calculated with (a) MOX-07 and (b) CRG potentials. These contribution are compared with the relative lattice parameter calculated from the simulated XRD.

The sum of all the contribution fits quite nicely the expansion calculated from the simulated XRD patterns for both empirical potentials. For both cases, the main contribution of the expansion arises from the uranium interstitials followed by the oxygen vacancies, and for MOX-07 the Frank loops plays also an important part of the expansion. It is worth noticing that this finding is different from what has been previously reported in UO_2 by Chartier *et al.* [8] or by Jin *et al.* [9] who calculated this expansion comparison with another empirical potential and did not take into account the oxygen defect contributions. Moreover, in their study, the values of the relaxation volumes were also different especially for the uranium vacancy for

which the relaxation volume is positive. Nevertheless, the main contribution of the expansion remains the cation interstitials.

The swelling of the material under irradiation can also be directly measured experimentally by the volume increase of the irradiated sample. Identical procedure can be applied to our MD boxes. We measure directly the box expansion as a function of increasing dose. Figure 8(a) reports this evolution. For comparison the expansion calculated from XRD are also displayed in the same graph.

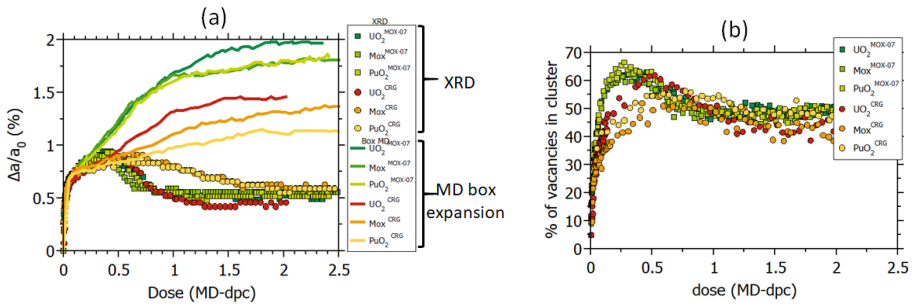

Figure 8: (a) Evolution of the relative lattice parameters [a(MD-dpc)-a(0)]/a(0) as a function of irradiation dose calculated from the simulated XRD pattern (symbols) and from the direct expansion of the simulation MD boxes (straight lines). (b) Evolution of the percentage of vacancies embedded in vacancy cluster of minimum size 3 as a function of irradiation dose. Both graphs report the results for UO_2, (U,Pu)O_2 solid solution noted MOx, and PuO_2 calculated with the MOX-07 and CRG potentials.

Differences between both types of measurement appear clearly. For the doses corresponding to the point defect regime (*i.e.* area in pink in figures 1 and 2) the expansion is identical. However, for higher doses corresponding to what we have referred as the dislocation regime (*i.e.* area in blue and grey in figures 1 and 2) the expansion calculated directly with the MD box

continues to increase and reaches a plateau after approximatively 1 MD-dpc. This behaviour does not correlate with the theoretical expansion calculated with the equation 4. Nonetheless, it seems to correspond with the evolution of the vacancy densities reported in figures 1 and 2. Furthermore, vacancy clustering analysis, namely the number of vacancies that are embedded into vacancy cluster larger than bi-vacancies, shows that up to 30% of the vacancies are not isolated at high doses, see figure 8(b). The maximum size of these vacancy clusters is found to be between 30 to 50 vacancies corresponding to nanocavities of 1 to 1.5 nm diameter. We believe that this is these nanocavities that impose the MD box to swell but their influence does not appear in the expansion of the XRD pattern because it does not affect much the surrounding matrix lattice parameter.

4. Conclusions

Molecular dynamics simulations have been carried out to investigate the evolution with irradiation dose of the microstructure of (U,Pu)O_2 solid solutions. Irradiation damage is created using the Frenkel pair accumulation method and assessed with two empirical potentials. One, MOX-07, gives good results on the point defects formation energy; while the other, CRG, provides better results on the mechanical properties. Overall, both potentials provide the same behaviour even if the CRG potential is influenced more by the presence of Pu content.

Along the irradiation pathway, each microstructure created with spontaneous reorganization of defects is analysed directly by determining the point defects and dislocation densities and by calculating the X-Ray diffraction

patterns. Since the atomic configuration is well defined within the molecular dynamics simulations, correlation between the simulated X-Ray diffraction patterns and the microstructure evolution could be established. This provides a database, which can help the interpretation and/or to deconvolve the experimental XRD patterns of real physical irradiated MOx.

Unsurprisingly, we found that the full width at half maximum of the XRD peaks are directly correlated to the perfect dislocation loop density. The increase of the FWHM corresponds usually to an increase of the microstrain, which is related herein to the creation of small disoriented nanodomains. More unexpected, small peaks appear on the simulated XRD patterns for intermediate irradiation doses and seem directly correlated to the Frank loop density. These small peaks represent in our simulation the track of a fluorite-like structure embedded within the Frank loops. Moreover, this structure-like has a smaller lattice parameter and corresponding to fluorite structure under compression stress. This needs to be confirmed, yet it could be a method to measure the Frank loop density, which is hard to characterize experimentally due to the small sizes of these loops.

Finally, the swelling under irradiation have been investigated. The dilatation found with the XRD pattern mainly originates from the presence of the cation interstitials and the oxygen vacancies and to a lesser extent from the frank loop density when it exists. However, the dilation calculated directly from the dimension of the simulation box is mainly due to the creation of nanocavities.

Acknowledgements

This research is part of the INSPYRE project, which has received funding from the Euratom research and training programme 2014-2018 under Grant Agreement No 754329. This research contributes to the joint programme on nuclear materials (JPNM) of the European energy research alliance (EERA). This work was granted access to the HPC resources of [TGCC] under the allocation 2020-mtt7073 made by GENCI.

References

[1] N. Ishikawa, T. Sonoda, Y. Okamoto, T. Sawabe, K. Takegahara, S. Kosugi, A. Iwase, "X-ray study of radiation damage in UO2 irradiated with high-energy heavy ions", J. Nucl. Mater., 419 (2011) 392-396.

[2] C. Mieszczynski, G. Kuri, C. Degueldre, M. Martin, J. Bertsch, C.N. Borca, D. Grolimund, Ch. Delafoy, E. Simoni, "Irradiation effects and micro-structural changes in large grain uranium dioxide fuel investigated by micro-beam X-ray diffraction", J. Nucl. Mater., 444 (2014) 274-282.

[3] T-H. Nguyen, A. Debelle, A. Boulle, F. Garrido, L. Thomé, V. Demange, "Mechanical response of UO2 single crystals submitted to low-energy ion irradiation", J. Nucl. Mater., 467 (2015) 505-511.

[4] E. De Bona, A. Benedetti, O. Dieste, D. Staicu, T. Wiss, R.J.M. Konings, "Radiation effects in alpha-doped UO2", Nucl. Instrum. Methods Phys. Res B, 468 (2020)54-59.

[5] A. Boulle, A. Chartier, A. Debelle, X. Jin, and J.-P. Crocombette, "Computational diffraction reveals long-range strains, distortions and disorder in molecular dynamics simulations of irradiated single crystals", J. Appl. Cryst., 55 (2022) 296-309.

[6] A. Debelle, A. Boulle, A. Chartier, F. Gao, and W. J. Weber, "Interplay between atomic disorder, lattice swelling, and defect energy in ion-irradiation-induced amorphization of SiC", Phys. Rev. B 90 (2014) 174112.

[7] A. Boulle, A. Chartier, J-P. Crocombette, T. Jourdan, S. Pellegrino, A. Debelle, "Strain and damage build-up in irradiated crystals: Coupling X-ray diffraction with numerical simulations", Nucl. Instrum. Methods Phys. Res. B, 458 (2019) 143-150.

[8] A. Chartier, C. Onofri, L. Van Brutzel, C. Sabathier, O. Dorosh, and J. Jagielski, "Early stages of irradiation induced dislocations in urania", Appl. Phys. Lett., 109 (2016) 181902.

[9] X. Jin, A. Boulle, A. Chartier, J-P. Crocombette, A. Debelle, "Analysis of strain and disordering kinetics based on combined RBS-channeling and X-ray diffraction atomic-scale modelling", Acta Materialia, 201 (2020) 63-71.

[10] F. Bruneval, M. Freyss, and J-P. Crocombette, "Lattice constant in non-stoichiometric uranium dioxide from first principles", Physical Review Materials, 2 (2018) 023801.

[11] A. Chartier, C. Meis, J. P. Crocombette, W.J. Weber, and L. R. Corrales, "Molecular Dynamic Simulation of Disorder Induced Amorphization in Pyrochlore", Phys. Rev. Lett., 94 (2005) 25505.

[12] J.P. Crocombette, A. Chartier, and W.J. Weber, "Atomistic simulation of amorphization thermokinetics in lanthanum pyrozirconate", Appl. Phys. Lett., 88 (2006) 051912.

[13] S. Plimpton, Fast Parallel Algorithms for Short-Range Molecular Dynamics, J Comp Phys, 117 (1995) 1-19. https://lammps.sandia.gov/index.html

[14] A. Chartier, L. Van Brutzel, P. Fossati, Ph. Martin, and C. Guéneau (2020). "Thermodynamic and Thermophysical Properties of the Actinide Oxides". In: Konings, Rudy JM and Stoller Roger E (eds.) Comprehensive Nuclear Materials 2nd edition, vol. 7, pp. 111–154. Oxford: Elsevier.

[15] S.I. Potashnikov, A.S. Boyarchenkov, K.A. Nekrasov, A.Ya. Kupryazhkin, "High-precision molecular dynamics simulation of UO2–PuO2: Pair potentials comparison in UO2", J. Nucl. Mater., 419 (2011) 217-225.

[16] H. Balboa, L. Van Brutzel, A. Chartier, and Y. Le Bouar, "Assessment of empirical potential for MOX nuclear fuels and thermomechanical properties", J. Nucl. Mater., 495 (2017) 66-77.

[17] H. Balboa, L. Van Brutzel, A. Chartier, and Y. Le Bouar, "Damage

525 characterization of (U,Pu)O2 under irradiation by Molecular Dynamics
526 simulations", accepted in J. Nucl. Mater., 512 (2018) 440-449.

527 [18] M.W.D. Cooper, M.J.D. Rushton, and R.W. Grimes, "A many-body
528 potential approach to modelling the thermomechanical properties of ac-
529 tinide oxides", J. Phys. Condens. Matter., 26 (2014) 105401.

530 [19] M.W.D. Cooper, S.T. Murphy, M.J.D. Rushton, R.W. Grimes, "Ther-
531 mophysical properties and oxygen transport in the (UxPu1-x)O2 lat-
532 tice", J. Nucl. Mater., 461 (2015) 206-214.

533 [20] D. Bathellier, M. Lainet, M. Freyss, P. Olsson, E. Bourasseau, "A new
534 heat capacity law for UO2, PuO2 and (U,Pu)O2 derived from molecular
535 dynamics simulations and useable in fuel performance codes", J. Nucl.
536 Mater., 549 (2021) 152877.

537 [21] Hockney and Eastwood, Computer Simulation Using Particles, Adam
538 Hilger, NY (1989)

539 [22] L. Van Brutzel, A. Chartier, J.-P. Crocombette, "Basic mechanisms
540 of Frenkel pair recombinations in UO2 fluorite structure calculated by
541 molecular dynamics simulations", Phys. Rev. B, 78 (2008) 024111.

542 [23] H.J.C. Berendsen, J.P.M. Postma, W.F. van Gunsteren, A. DiNola, and
543 J.R. Haak, "Molecular dynamics with coupling to an external bath", J.
544 Chem. Phys., 81 (1984) 3684.

545 [24] A. Stukowski, K. Albe, "Visualization and analysis of atomistic simula-
546 tion data with OVITO - the Open Visualization Tool", Modelling Simul.
547 Mater. Sci. Eng., 18 (2010) 015012, http://ovito.org/

[25] P. fossati, personal communication.

[26] Wojdyr, Debyer sofware, 2008. https://debyer.readthedocs.io/en/latest/#usage

[27] M. Parrinello and A. Rahman, "Polymorphic transitions in single crystals: A new molecular dynamics method", J. Appl. Phys., 52 (1981) 7182-7190.

[28] M. Wojdyr, "*Fityk*: a general-purpose peak fitting program", J. Appl. Cryst., 43 (2010) 1126-1128.

[29] H. Matzke, "Radiation enhanced diffusion in UO2 and (U,Pu)O2", Radiation Effects 75 (1983) 317.

[30] T. Sekine and T. Aoyama, Proceedings of the Monte-Carlo 2000 Conference p.737.

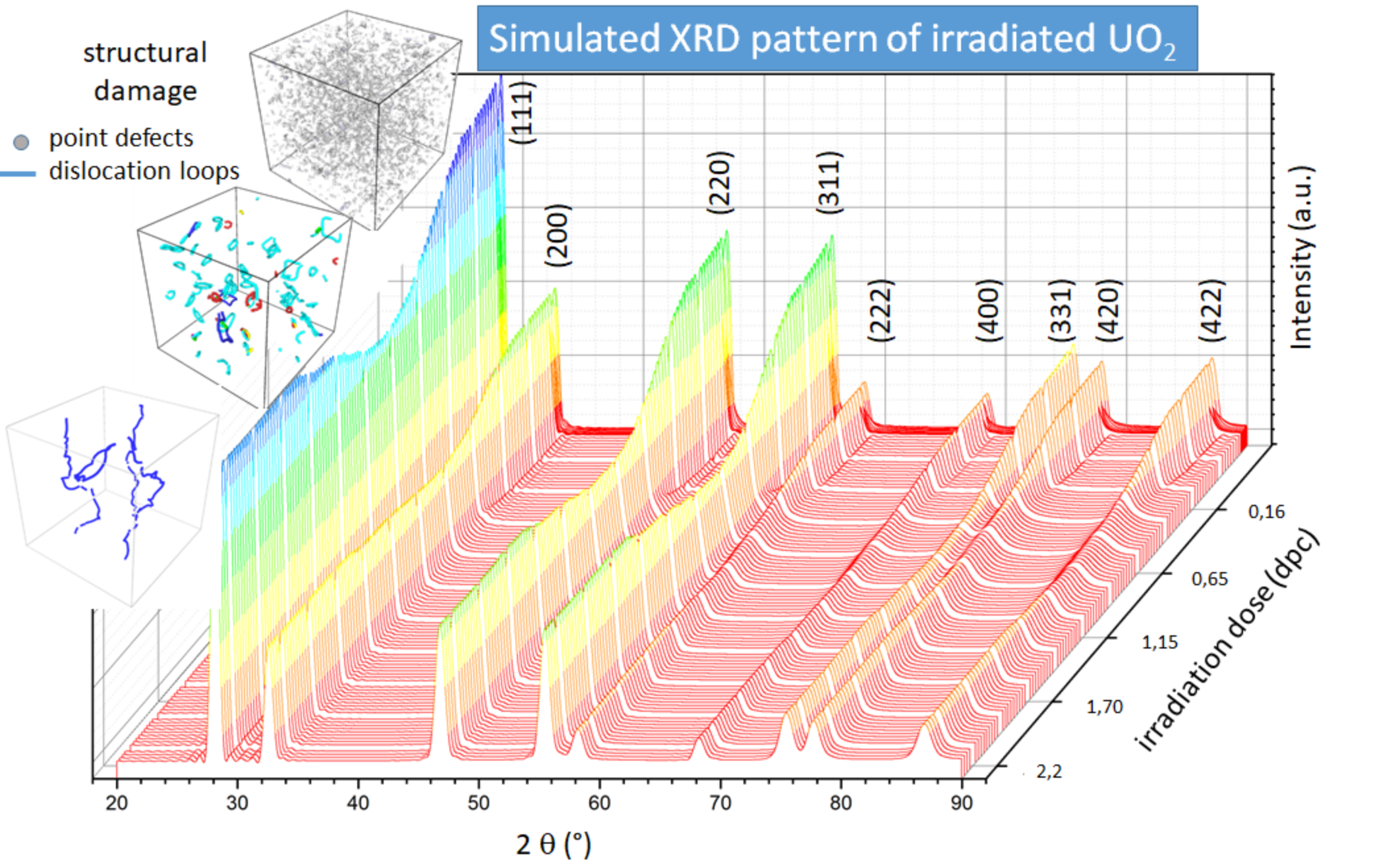
Simulated XRD pattern of irradiated UO_2
structural damage
point defects
dislocation loops
(111)
(200)
(220)
(311)
(222)
(400)
(331)
(420)
(422)
Intensity (a.u.)
irradiation dose (dpc)
0,16
0,65
1,15
1,70
2,2
20
30
40
50
60
70
80
90
2 θ (°)